ISSN (Print) 1226-1750
ISSN (Online) 2233-6656
Journal of Magnetics 27(1), 7-17 (2022) https://doi.org/10.4283/JMAG.2022.27.1.007

Effect of Mn doping on the Structural, Dielectric, and Multiferroic Properties of $BiFeO_3$-$BaTiO_3$ Ceramics Fabricated by Spark Plasma Sintering

Meng Wang[1]* and Zengxu Xu[2]

[1]*School of Mechanical and Electrical Engineering, Shenzhen Polytechnic, Shenzhen 518055, China*
[2]*Department of Physics, Southern University of Science and Technology, Shenzhen 518055, China*

(Received 23 September 2021, Received in final form 8 March 2022, Accepted 16 March 2022)

0.67$BiFeO_3$-0.33$BaTiO_3$-xwt%Mn ceramics were synthesized using the SPS method. Fine $BiFeO_3$-$BaTiO_3$ ceramics with a morphotropic phase boundary were formed, as demonstrated by XRD and SEM. The dielectric constants reached approximately 4000. The ferroelectric properties of Mn-doped $BiFeO_3$-$BaTiO_3$ were significantly improved compared with undoped $BiFeO_3$-$BaTiO_3$. The highest magnetic properties were obtained when the sintering temperature was 820 °C and the doping content was 0.3 wt%, and were superior to those fabricated using other methods. The Mn-doped $BiFeO_3$-$BaTiO_3$ multiferroic ceramic synthesized in this work shows promise for application in data storage.

Keywords : multiferroic, $BiFeO_3$-$BaTiO_3$, spark plasma sintering, Mn doping

1. Introduction

In recent years, multiferroic ceramics has become an area of research focus in the development of next-generation information systems. In order to overcome the health threat and pollution problems of $Pb(Zr,Ti)O_3$ ceramics, Pb-free $BiFeO_3$ ceramics became widely studied, and some breakthroughs were realized. $BiFeO_3$ has demonstrated its uniqueness in being a material that possesses ferroelectric and ferromagnetic properties at ambient temperature [1]. In addition, Bi^{3+} in $BiFeO_3$ has a lone electron pair, which is similar to the electron configuration of Pb^{3+} in $Pb(Zr,Ti)O_3$, which indicates its potential as a replacement for traditional Pb-containing multiferroic ceramics [2]. While some fundamental problems of $BiFeO_3$ ceramics need to be solved, the foremost problem is the evaporation problems of Bi ions during the fabrication process. Three main unfavorable outcomes should be considered. The first is stoichiometric changes, which will lead to high leak current and impair the ferroelectric properties of $BiFeO_3$ ceramics. The second is that poisonous Bi can leak into the air, which deteriorates human health. The last is that Bi evaporation will pollute the sintering and testing machines [3, 4]. Therefore, effective methods must be adopted to address these outcomes.

One popular solution is the combination of ABO_3 ceramics with single-phase $BiFeO_3$. Of all the additive ABO_3 ceramics, $BaTiO_3$ is the most extensively investigated. The current research shows that the ferroelectric and piezoelectric properties are significantly improved for $BiFeO_3$-$BaTiO_3$ ceramics compared to single-phase $BiFeO_3$ [5, 6]. Moreover, morphotropic phase boundaries are formed once the molar percentage of $BaTiO_3$ is higher than 0.67. Therefore, the solid solution structure will change from having a diamond cubic phase to tetragonal phase. At this point, a sudden increase in ferroelectric and piezoelectric properties can be achieved while maintaining magnetization, providing a valid solution for bottleneck issues in ceramic manufacturing.

In order to further improve the overall properties of $BiFeO_3$-$BaTiO_3$, a third component should be added. The main additive components are various metal oxides. For instance, MnO_2 can enhance the resistivity of the ceramics, while CuO can also be used as a magnetic refiner. The benefit of MnO_2 is that it can also adjust the turning point of morphotropic phase boundaries [7].

The preparation process of $BiFeO_3$-$BaTiO_3$ ceramics mainly includes precursor powder preparation and high-temperature sintering. The precursor powders are mainly prepared using the solid-phase method, high-energy ball

©The Korean Magnetics Society. All rights reserved.
*Corresponding author: Tel: +86-755-26731137
Fax: +86-755-26731137, e-mail: wangmeng04@szpt.edu.cn

© 2022 Journal of Magnetics

milling method, or dissolution gel method. The sintering process is composed of spark plasma sintering, hot pressing, partial coprecipitation, coating, template grain growth, microwave sintering, and mechanochemical synthesis [8, 9]. Although the traditional solid-state reaction is an economical and effective method with which to prepare ceramics, there are many factors in the preparation process, such as the sintering time, sintering temperature, ball milling time, ball milling speed, pre-sintering temperature, and ball material used. These factors affect the size of the grains in the precursor powder, which determines the properties of the ceramics. If the size of the powder is too large, obvious cracks or pores can be detected in the microstructure of the sintered ceramics. However, this does not mean that the smaller the powder, the better the performance. In addition, when oxide is used as the starting material and $BiFeO_3$ bulk ceramics are prepared using the conventional solid-state synthesis method, a large number of impurities ($Bi_2Fe_4O_9$, $Bi_{25}FeO_4$, and Bi_2O_3) are formed. The formation of impurities can be effectively inhibited and the density increased using a wet chemical method along with appropriate oxide precursors. The existing methods for high-temperature sintering include traditional solid-phase sintering, liquid-phase sintering, and spark plasma sintering.

The sintering temperature of pure-phase $BiFeO_3$ is generally lower than 850 °C, and that of pure-phase $BaTiO_3$ is usually over 1350 °C. For the traditional sintering method, the sintering temperature of dual phase solid solution is generally between 800 and 1100 °C. Long periods of sintering at high temperatures will cause volatilization and a shift of Bi_2O_3 components in raw materials, and it is difficult to avoid the formation of minor impurities. By contrast, spark plasma sintering (SPS) is a new technology to prepare traditional and functional materials. SPS technology introduces pulse current into the sintered powder to spark the material such that ions are activated and local high-temperature sintering occurs. Uniform axial pressure is applied through the top and bottom pressure bars to rapidly transfer heat. The sintering temperature is lower than that for traditional sintering, and the sintering process is faster. This can effectively reduce the volatilization of Bi_2O_3 [10].

In this article, $0.67BiFeO_3$-$0.33BaTiO_3$ nanopowders were fabricated, and $0.67BiFeO_3$-$0.33BaTiO_3$ ceramics were subsequently obtained using SPS. The crystal structure of the solid solution with this content comprises morphotropic phase boundaries, which have the best piezoelectric and ferroelectric properties. Furthermore, appropriate MnO_2 content was added to further adjust the ferroelectric properties of ceramics. SPS processes were also adopted. The influence of MnO_2 content and sintering temperature on the dielectric and ferroelectric properties of the ceramics was extensively studied.

2. Experimental

$0.67BiFeO_3$-$0.33BaTiO_3$-x wt%Mn nanoparticles were synthesized using the traditional calcination method. The raw reagents adopted in the process were Bi_2O_3 (Aladdin, >99%), Fe_2O_3 (Aladdin, >99%), $BaCO_3$ (Aladdin, >99%), Ti_2O_3 (Aladdin, >99%), and $MnCO_3$ (Macklin, >99.5%). First, stoichiometric amounts of raw powders were ball milled separately with CH_3COOH at 10 hours, 400 r/min. Then, the milled powders were dried and mixed, milled again under the same conditions, and dried as precursors for the sintering. Therefore, $0.67BiFeO_3$-$0.33BaTiO_3$-0.15 wt%Mn, $0.67BiFeO_3$-$0.33BaTiO_3$-0.2 wt%Mn, and $0.67BiFeO_3$-$0.33BaTiO_3$-0.3 wt%Mn precursors were obtained in this way.

The SPS processing steps are as follows. The precursor powders placed in a special graphite die were separately heated to 720, 750, and 780 °C at a rate of 100 °C/min, then at 50 °C/min for 1 minute, and 25 °C/min for 2 minutes, followed by sintering for 5 min at 820, 850, and 880 °C, respectively, under a vacuum of 10^{-2} Pa. During the entire SPS process, a stable pressure of 50 MPa was constantly exerted on the samples. The pellets obtained after SPS with 10 mm diameter and 2 mm thickness were annealed at 650 °C for 4 hours to achieve more thorough reaction and a reduction in carbon contamination.

The crystal structures of the powers and ceramics were tested by X-ray diffraction (XRD) using a Rigaku diffractometer with Cu-Kα radiation (D/max-RB, Rigaku, Japan). The densities of the samples were examined by application of the Archimedes method using distilled water. Both the surface morphology of the powders and the fracture surface of the ceramics were tested by field emission scanning electron microscopy coupled with EDS (PhenomProX FE-SEM/EDS,USA). The electrical properties of the samples were measured using a dielectric analyzer (PSM1735, DMS-500, UK). The ferroelectric properties of the samples were obtained using a ferroelectric analyzer (Radiant Premier, USA). Magnetic properties were tested using a physical property measurement system (DynaCool-9T, Quantum Design, Leatherhead, Surrey, UK) operated at room temperature (298 K).

3. Results and Discussion

The ball milling nanopowders were characterized by XRD. The results show that the precursor powders are a

homogeneous mixture of Bi_2O_3, $BaCO_3$, Fe_2O_3, and Ti_2O_3, and the XRD characterization is shown in Fig. 1(a). As the maximum Mn doping content was lower than 0.3 wt%, the diffraction peak corresponding to Mn was not detected. Thus, there is no significant difference in the XRD analysis of the precursor powders with different Mn doping contents. The diffraction peaks of Bi_2O_3 and Fe_2O_3 are stronger than those of $BaCO_3$ and Ti_2O_3, as the raw materials were prepared according to stoichiometric $0.67BiFeO_3$-$0.33BaTiO_3$ with higher Bi and Fe contents.

The XRD analysis of the pellets obtained using SPS is shown in Fig. 1(b), (c), (d). This shows that there was a large amount of Bi remaining in the pellets, as the lowest sintering temperature was 820 °C, which is close to the melting point of Bi_2O_3. During the sintering process, part of Bi_2O_3 melted. As shown in Fig. 1(b), (c), (d), if the Mn doping amount was 0.15 wt%, the diffraction peak of Bi was the highest once the sintering temperature rose to 880 °C. When the Mn content was 0.2 wt%, the intensity of Bi peak was lower than that of other Mn doping samples for all sintering temperatures. In addition, when the Mn content was 0.3 wt%, the intensity of the Bi peak was higher than that of the $BiFeO_3$ peak. The results show that the samples prepared at different temperatures and Mn doping amounts contain a large amount of impure Bi, but the samples for which 0.2 wt% Mn was used for doping had relatively low Bi impurities for the different sintering temperatures. This shows that MnO_2 can reduce the amount of impure Bi that is formed, and the optimal amount of added MnO_2 is 0.2 wt%. If more MnO_2 is added, the mismatch of lattices between MnO_2 and $BiFeO_3$ will impair the positive effects of MnO_2; thus, more Bi impurities will develop.

The XRD pattern of SPS pellets after annealing are shown in Fig. 2. Compared with the sample before annealing, the impurities were effectively eliminated in the ceramic sample, and Bi peak observed in the original sample had disappeared completely. XRD analysis of the samples with different annealing temperatures and Mn doping contents shows that the samples contained both tetragonal $BiTiO_3$ and cubic $BiFeO_3$, and morphotropic phase boundaries were formed in the samples. At the same annealing temperature, the samples for which 0.2 wt% Mn was used in doping had the least amount of

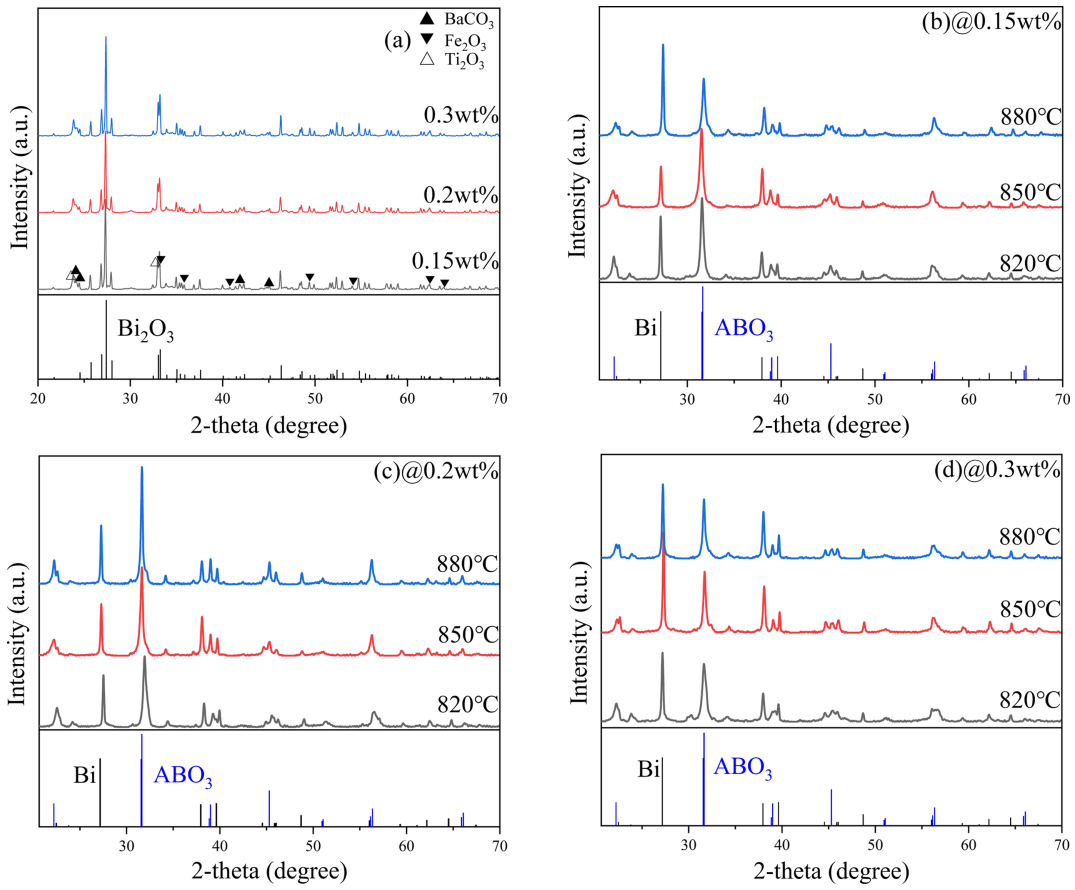

Fig. 1. (Color online) (a) XRD pattern of ball milling precursor powder; (b), (c), (d) samples sintered at different temperatures with the same amount of Mn doping (b, c and d are 0.15 wt%, 0.2 wt% and 0.3 wt% respectively).

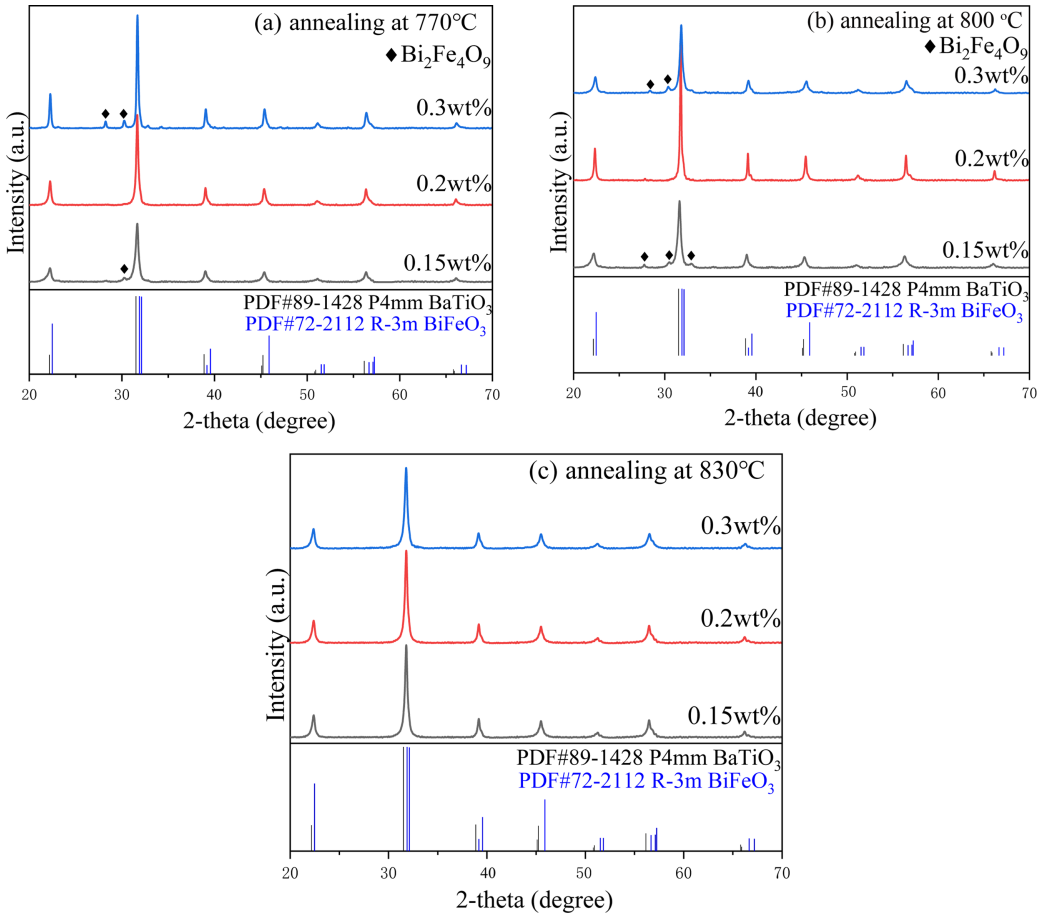

Fig. 2. (Color online) XRD patterns of sintered samples with Different Mn doping amount after annealing at (a) 770 °C, (b) 800 °C (c) 830 °C.

impurity phases and the highest purity, while other samples with different Mn contents had some impurity phases, which were analyzed as $Bi_2Fe_4O_9$. Fig. 2(c) shows the XRD patterns of the samples with different amounts of doped Mn after annealing at 830 °C. Here, the minor peaks observed in the samples at other annealing temperatures have disappeared.

In addition to reducing the purity of ceramics by adjusting the annealing temperature, it was also tested whether the purity change in samples with different Mn doping contents is different at the same annealing temperature. When the Mn content was 0.2 wt%, the purity of the sample was the highest, for which no impurity phase was observed, in contrast to samples with other amounts of Mn, where a small traces of impurity could be seen. Therefore, doping with an appropriate amount of Mn can reduce the formation of impurities after annealing.

Figure 3 shows the density of SPS samples after sintering at different temperatures. The density of the sample with a low sintering temperature was higher at the same Mn doping content, and the sample where 0.2 % Mn was used for doping had the highest density at a sintering temperature of 820 °C. The reason why a high sintering temperature does not increase the density of the

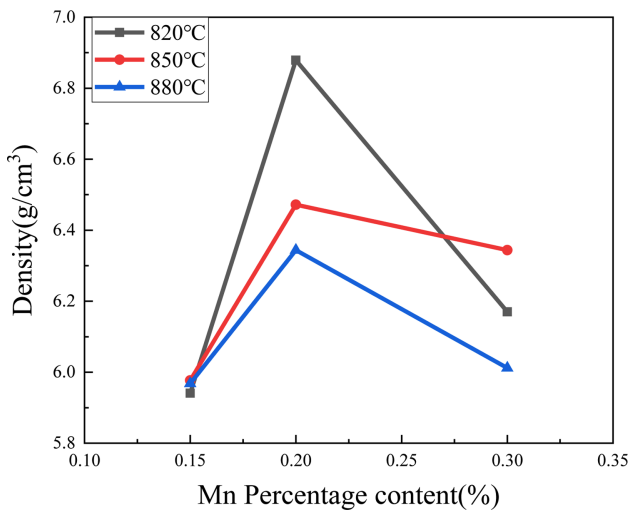

Fig. 3. (Color online) The density of SPS samples after sintering at different temperatures.

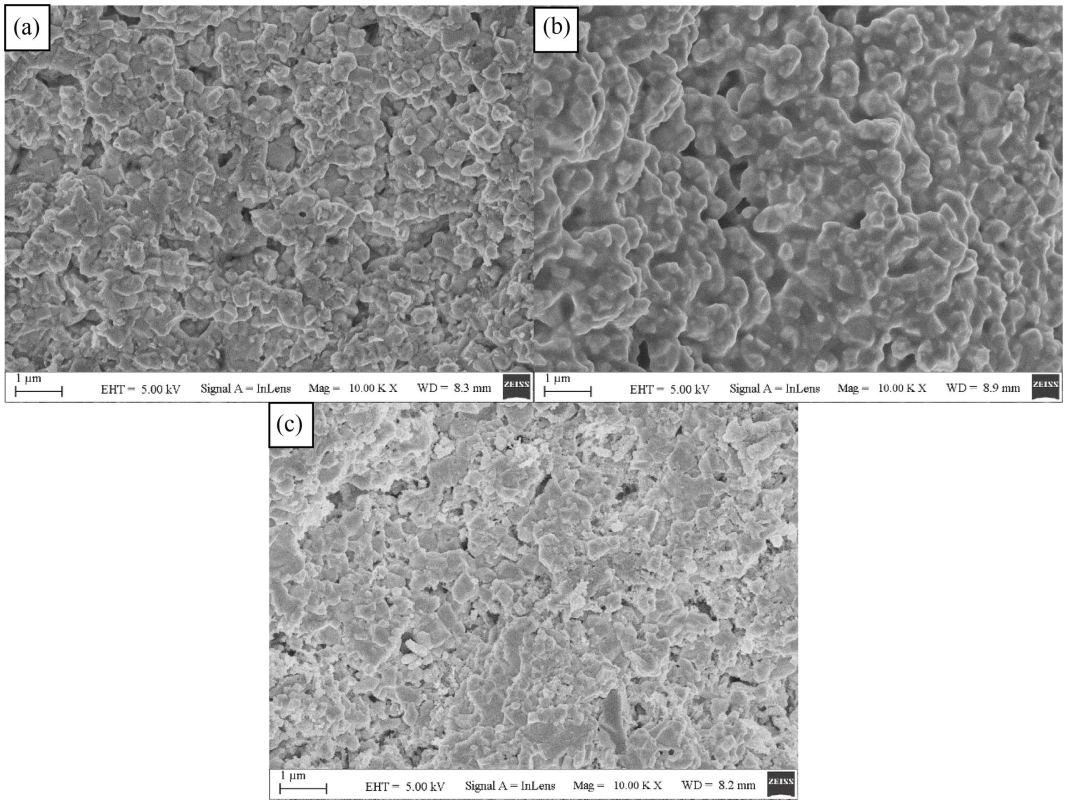

Fig. 4. SEM images of cross section of samples with different Mn content at 820 °C (0.15 wt%, 0.2 wt%, 0.3 wt% respectively).

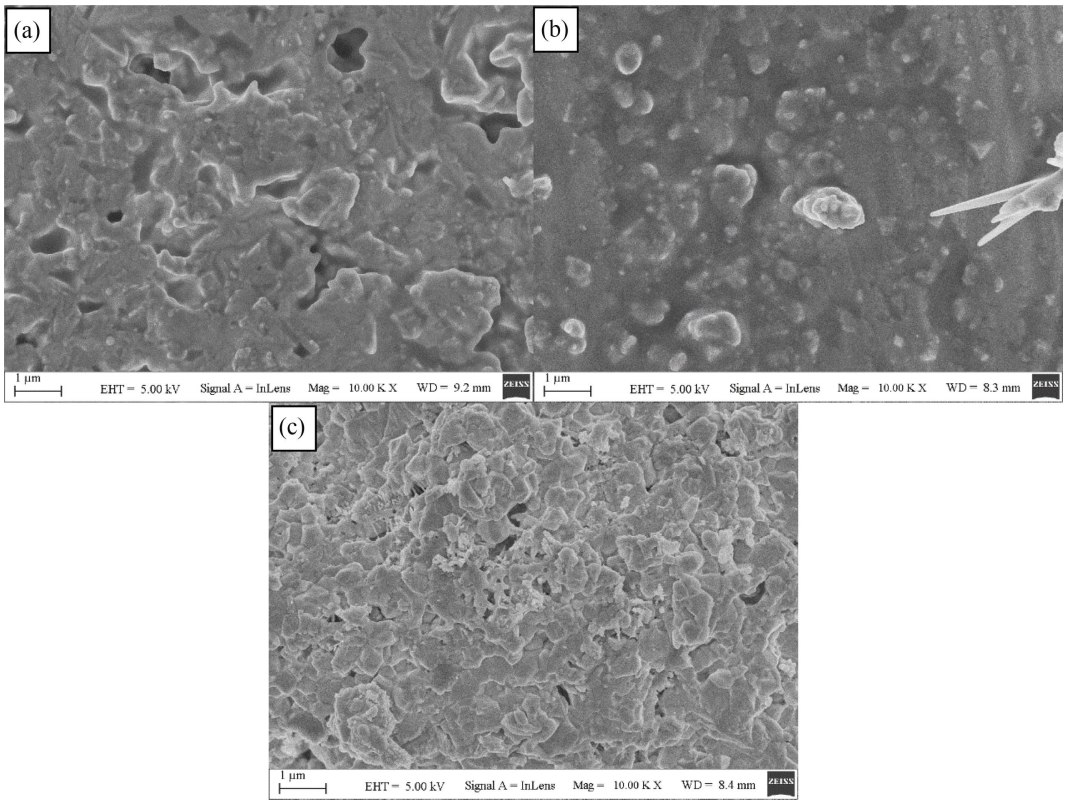

Fig. 5. SEM images of cross section of samples with different Mn content at 850 °C (0.15 wt%, 0.2 wt%, 0.3 wt% respectively).

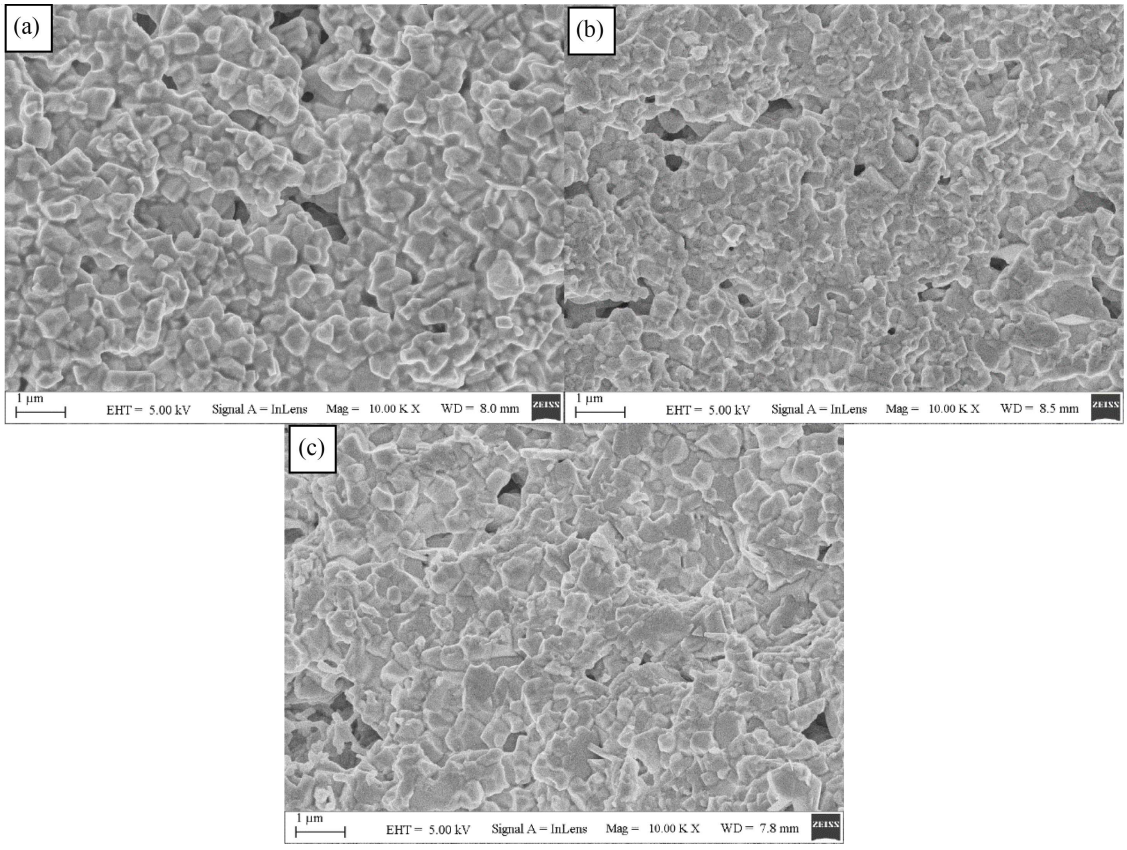

Fig. 6. SEM images of cross section of samples with different Mn content at 880 °C (0.15 wt%, 0.2 wt%, 0.3 wt% respectively).

ceramics may be that Bi_2O_3 melts to form a liquid phase during sintering, which hinders the contact of grains and forms many holes in the ceramics, thus reducing the density.

Figure 4-6 are the cross-sections of samples with different Mn contents produced at 820, 850, and 880 °C sintering temperatures. For the sample produced at 850 °C, there were almost no obvious single grains in the cross-section. The results show that with the increase in Mn content, the grain shape of the ceramic samples sintered at the same temperature changed to a crystal shape, which may be attributed to the Mn doping-assisted grain growth.

Figure 7 shows the temperature dependence of the dielectric constant of different Mn-doped ceramics at 1 MHz versus sintering temperature. At sintering temperatures of 820 and 850 °C, the dielectric constant of 0.2 wt% Mn-doped ceramics was the highest, and the dielectric loss was the lowest; thus, these dielectric properties are the best. The dielectric constant at room temperature was 359 and 407, respectively, which is higher than 143 of pure phase $BiFeO_3$. Second, the room temperature dielectric constant of 0.15 and 0.3 wt% Mn-doped ceramics was more than 200. The increase in the dielectric constant is due to the formation of morphotropic phase boundaries between $BaTiO_3$ and $BiFeO_3$. The energy at the phase boundary decreased, and the polarization of the material increased, which caused the dielectric constant to appear at the peak point in the phase boundary. In addition, an appropriate amount of Mn doping can inhibit Bi volatilization, reduce oxygen vacancies, and reduce leakage current. When the sintering temperature was 880 °C, the dielectric properties of the ceramics decreased with the increase in the amount of Mn used in doping.

Figure 8 shows the dielectric properties of different Mn-doped samples sintered at 820 °C. The dielectric constant of samples with different Mn doping amounts increased with the increase in sintering temperature. At a low temperature, the increasing rate of the dielectric constant was slow. At a high temperature, the increase rate of the dielectric constant was higher, and frequency dispersion occurred near 250 °C. The dielectric peak of samples with different Mn doping contents in the range of measured temperatures shows that the Curie temperature was higher than 450 °C. The dielectric constant of the sample changed rapidly with the doping amount of Mn at 0.15 wt%, and the dielectric dispersion was not obvious compared with other doping amounts. The dielectric loss

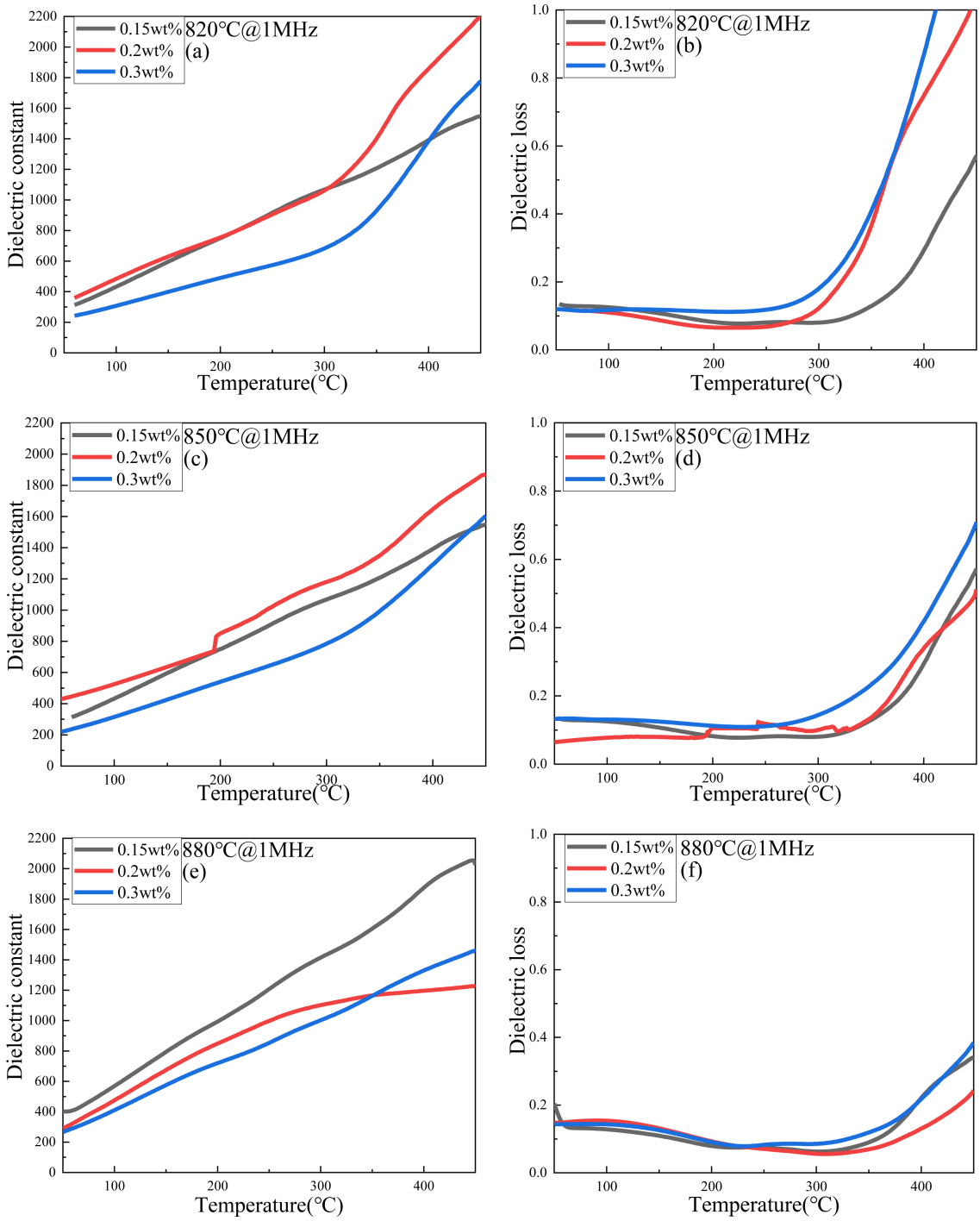

Fig. 7. (Color online) Relation of dielectric properties and temperature of samples with different Mn doping amounts at 1 MHz frequency: (a), (c), (c) the temperature dependence curves of dielectric constant at 820, 850, and 880 °C sintering temperatures, respectively; (b), (d), (f) the temperature dependence curves of dielectric loss at 820, 850, and 880 °C sintering temperatures, respectively.

of samples with different Mn doping amounts increased with the increase in temperature. Similarly, the sample of 0.2 wt% Mn sintered at 820 °C showed the best dielectric properties, as it has the lowest impurities and a comparatively low temperature was used, thus $BiFeO_3$ melting was avoided.

Figure 9 shows the ferroelectric hysteresis loops, measured at room temperature, of Mn-doped $BiFeO_3$-$BaTiO_3$ ceramics sintered at 820 °C. It can be seen from the figure that the ferroelectric properties of the sample

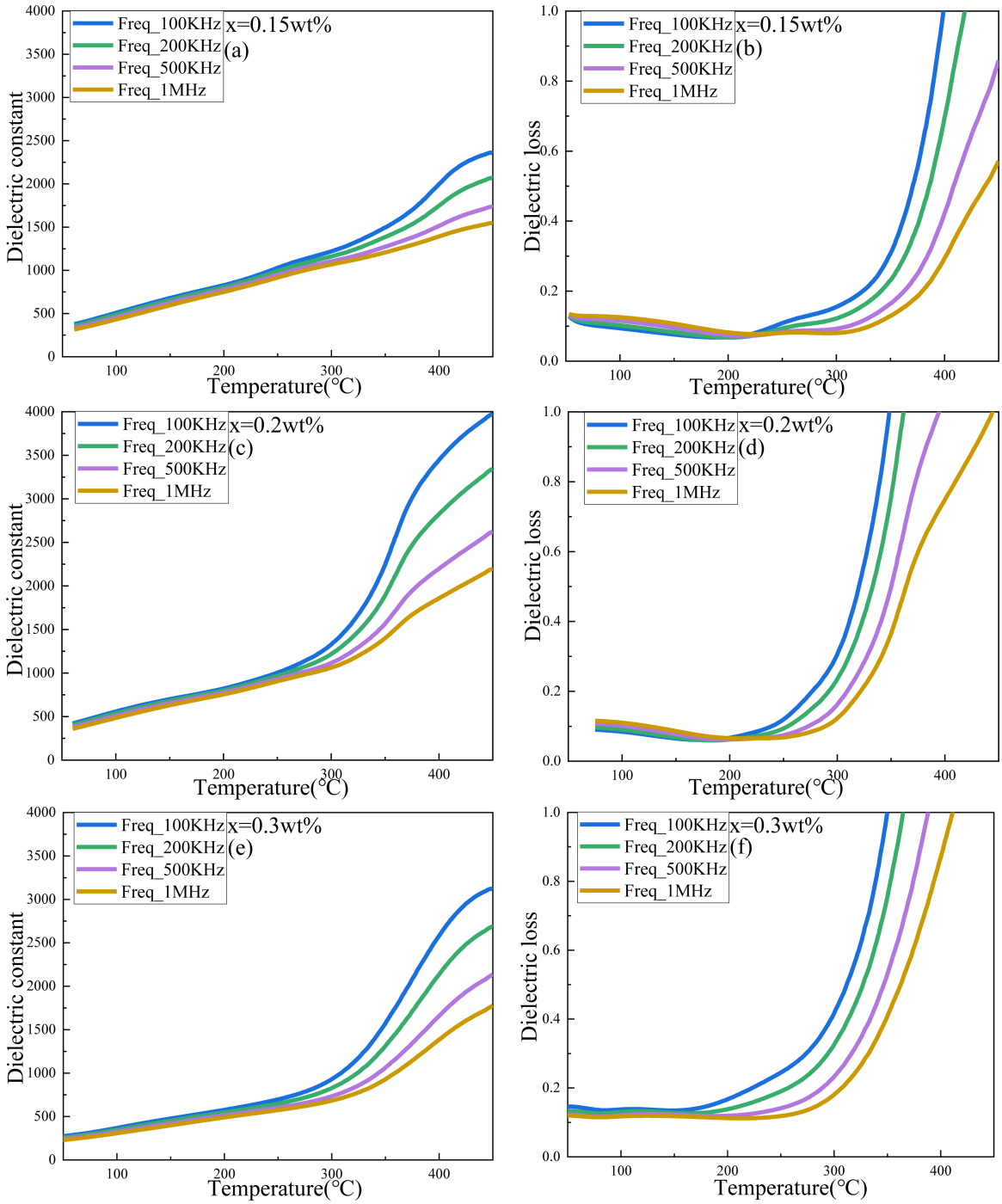

Fig. 8. (Color online) Temperature dependence of dielectric properties of Mn-doped samples sintered at 820 °C: (a), (c), (e) the temperature dependence curves of dielectric constant with Mn doping amounts of 0.15, 0.2, and 0.3 wt%, respectively. (b), (d), (f) the temperature dependence of dielectric loss with Mn doping amounts of 0.15%, 0.2%, and 0.3 wt%, respectively.

are poor, showing the emergence of large leakage current. The emergence of leakage current is closely related to the volatilization of bismuth and the generation of oxygen vacancies and Fe ions during the sintering process. As annealing was carried out in air, the oxygen vacancies caused by sintering cannot be effectively reduced. In addition, Mn doping introduces more divalent manganese ions, which can result in the reduction of Fe ions from trivalent to divalent in the sintering process, such that trivalent Fe ions are replaced by divalent Fe ions in the crystal structure of the sintered samples, resulting in a change in crystal structure. The above two reasons explain

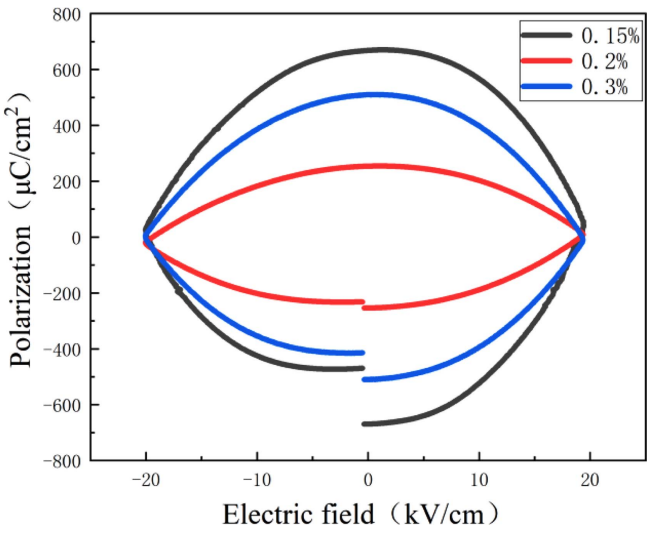

Fig. 9. (Color online) Ferroelectric hysteresis loops of samples with different Mn doping contents at 820 ℃ sintering temperature.

the emergence of large leakage current in the sintered samples, which results in their poor ferroelectric properties, while with the increase in Mn doping amount, the opening of the hysteresis loop first decreases and then increases. It can be seen that the remnant polarization and coercive field of the ceramic sample first decreased and then increased with the increase in Mn doping amount. The sample where 0.2 wt% Mn was used in doping had the best ferroelectric properties, with the highest charge density measured at approximately 203 μC/cm^2. Compared with pure phase $BiFeO_3$, the main reason for this is the decrease in leakage current, which helps to improve the ferroelectric properties of $BaTiO_3$-doped $BiFeO_3$. The other reason for the fine ferroelectric properties may be the suppression in oxygen vacancy concentration resulting from the addition of Mn.

Figure 10 shows the ferromagnetic hysteresis loops and parameters of different Mn-doped ceramic samples. The hysteresis loops of all samples were not saturated. If the

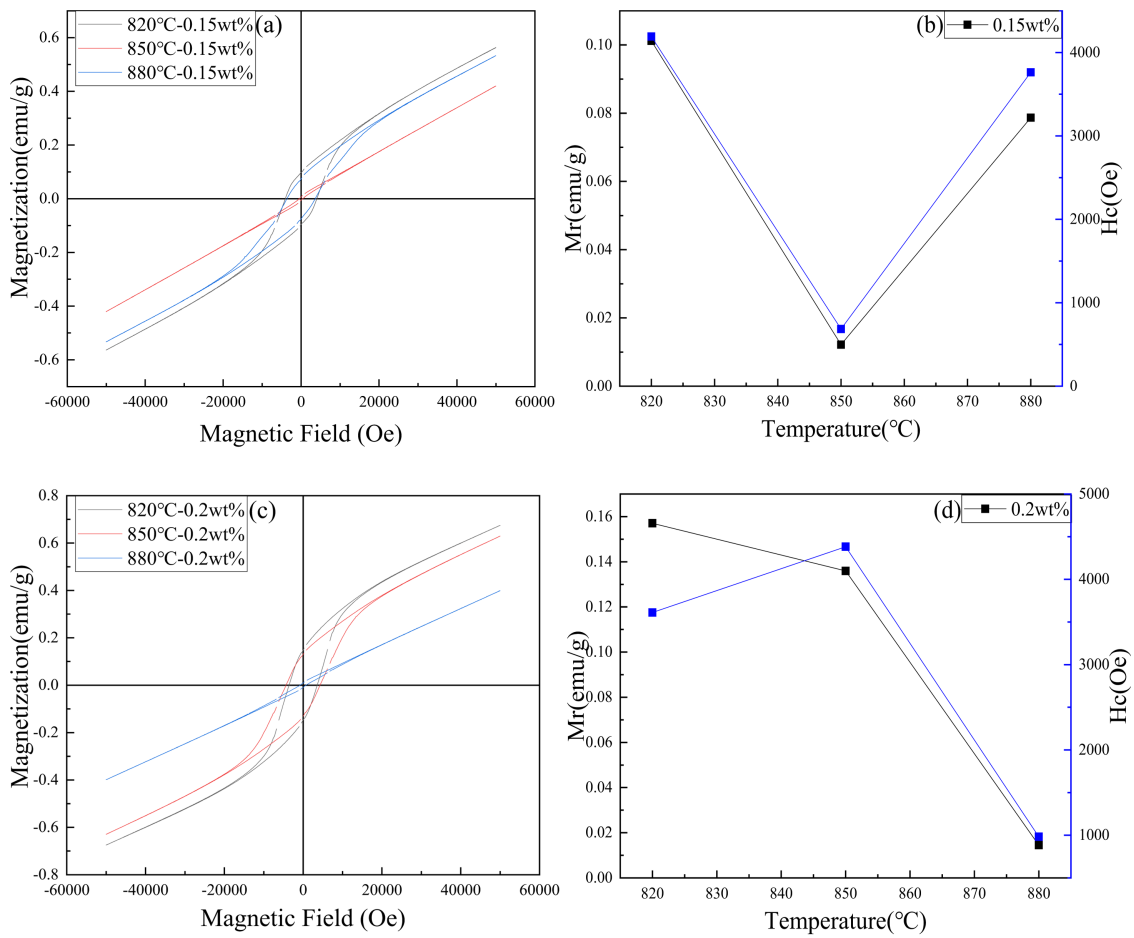

Fig. 10. (Color online) Magnetic properties of Mn-doped $BiFeO_3$-$BaTiO_3$ ceramics at different sintering temperatures: (a), (c) and (E) hysteresis loops with Mn contents of 0.15, 0.2, and 0.3 wt%, respectively. (b), (d), (f) magnetic parameters with Mn contents of 0.15, 0.2, and 0.3 wt%, respectively.

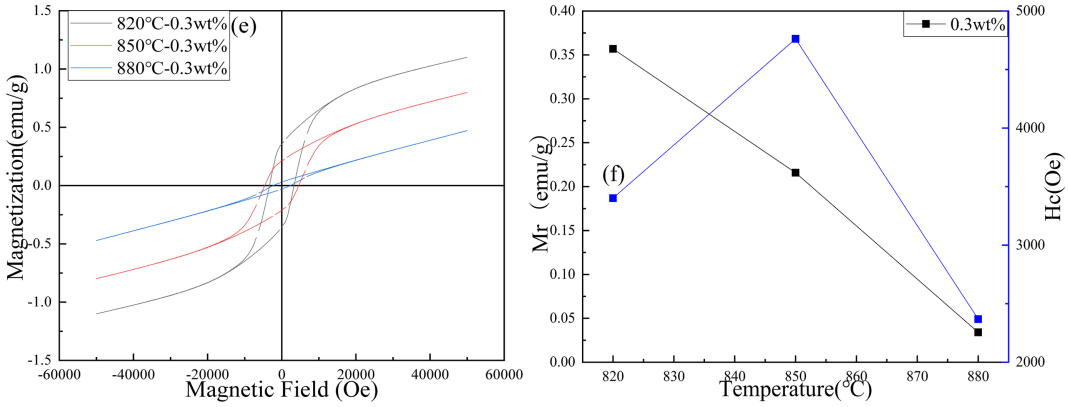

Fig. 10. Continued.

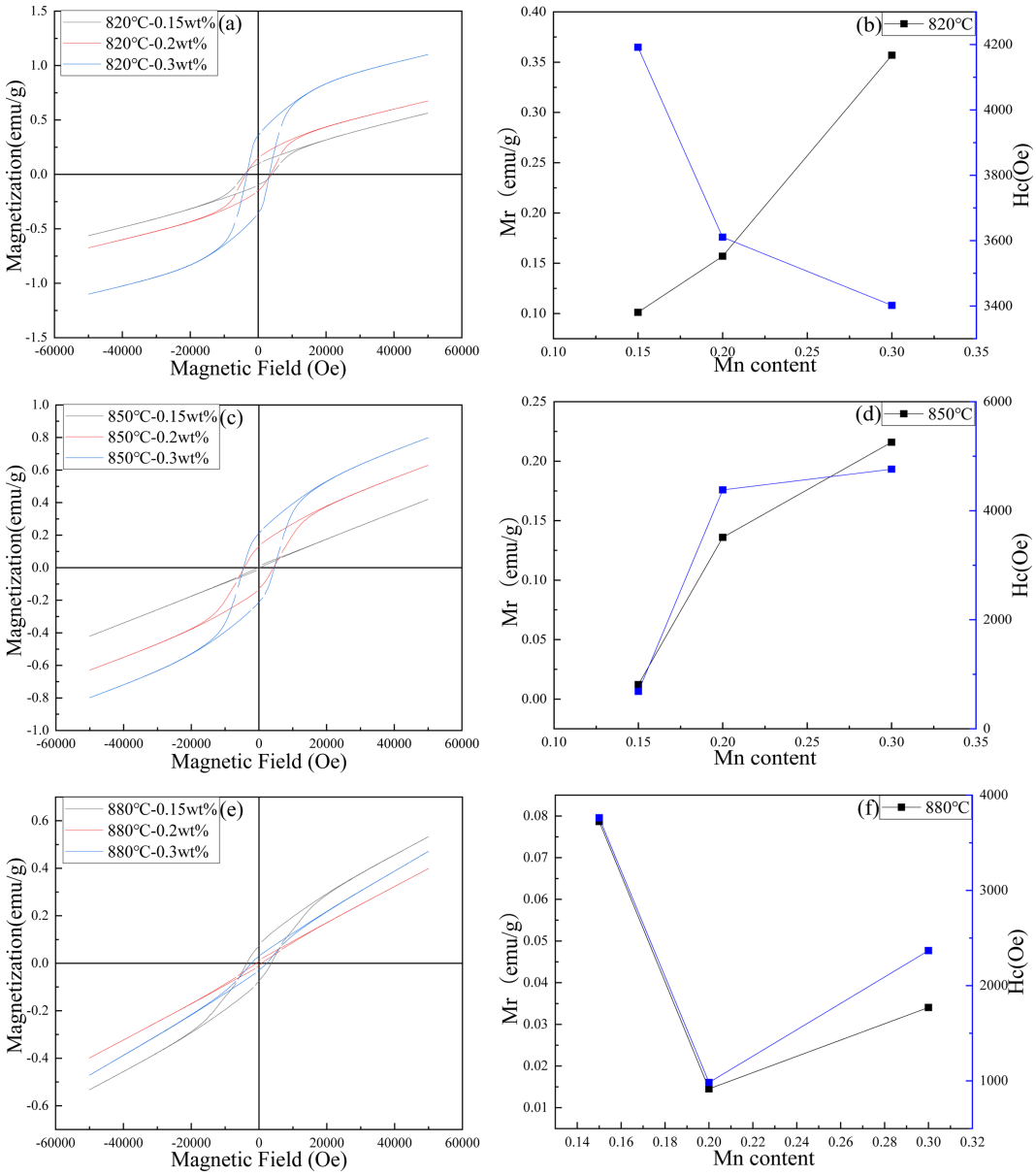

Fig. 11. (Color online) Magnetic properties of different Mn-doped $BiFeO_3$-$BaTiO_3$ ceramics: (a), (c) and (E) the hysteresis loops at 820, 850, and 880 °C, respectively. (b), (d) and (f) magnetic parameters at 820, 850, and 880 °C, respectively.

doping content was 0.15 wt%, and the sintering temperature was 820 °C, the remnant magnetization (MR) was 0.1012 emu/g and the coercive field (EC) was 419 Oe. If the doping content was 0.2 and 0.3 wt%, the remnant magnetization was 0.1571 and 0.3569 emu/g, respectively, and the coercive field was 3610 and 3401 Oe, respectively. Therefore, it is shown that the magnetic properties of $BiFeO_3$-$BaTiO_3$ ceramics are affected by sintering temperature and Mn doping content.

Figure 11 shows the hysteresis loops and main magnetic parameters of the magnetic properties of ceramic samples with Mn doping contents at a fixed sintering temperature. If the sintering temperature was 880 °C, the hysteresis loops of all samples with different doping contents were very unsaturated, and the remnant magnetization was less than 0.08 emu/g. If the Mn doping content was 0.2 wt%, the magnetic parameters were the lowest, the remnant magnetization was 0.0145 emu/g, and the coercive field was 982 Oe. If the sintering temperature was 820 °C, the magnetic properties of the sample were better than those of the other two temperatures, and the hysteresis loop tended to be saturated. At this sintering temperature, the sample with Mn doping of 0.3 wt% had the best magnetic properties, with remnant polarization of 0.3569 emu/g and a coercive field of 3401 Oe.

Previous studies have shown that high sintering temperature can cause Bi volatilization in $BiFeO_3$-$BaTiO_3$ ceramics, and the loss of Bi can increase the magnetic properties of the samples. Mn doping can inhibit the volatilization of Bi and reduce the magnetic properties of the ceramics. Mn doping can cause lattice distortion and enhance the magnetic properties of the ceramics. The melting point of Bi_2O_3 is 830 °C, so the samples sintered at 820 and 850 °C had little Bi volatilization. The magnetic properties were enhanced with the increase in the amount of Mn doping. A high sintering temperature of 880 °C will lead to Bi volatilization, thus reducing the magnetic properties of the final material. It is concluded that the magnetic properties of $BiFeO_3$-$BaTiO_3$ ceramics are affected by Mn doping amount and temperature. The best magnetic properties were obtained when the sintering temperature was 820 °C and the Mn doping content was 0.3 wt%.

4. Conclusion

Mn-doped $BiFeO_3$-$BaTiO_3$ ceramics were successfully prepared using spark plasma sintering. The crystal structure of $BiFeO_3$-$BaTiO_3$ ceramics showed a combination of tetragonal and trigonal phases, and a morphotropic phase boundary was formed. The dielectric constants of 0.15, 0.2, and 0.3 wt% Mn-doped samples were 238.391, 256.366, and 397.081, respectively. Compared with pure $BiFeO_3$, the doped ceramics had improved dielectric properties. Mn doping can be used to enhance the ferroelectric properties of $BiFeO_3$-$BaTiO_3$ ceramics, and the sample where 0.2 wt% Mn was used in doping had the best ferroelectric properties. These results show that the magnetic properties of $BiFeO_3$-$BaTiO_3$ ceramics are affected by Mn doping and temperature. The best magnetic properties were obtained when the sintering temperature was 820 °C and the Mn doping content was 0.3 wt%. This shows that Mn-doped $BiFeO_3$-$BaTiO_3$ ceramics are a promising multiferroic material for application in data storage.

Acnkowledgement

This work was supported by Young Innovative Talents Project of General Colleges and Universities in Guangdong Province (2019GKQNCX127) and the Post-Doctoral Later-Stage Foundation Project of Shenzhen Polytechnic (6020271008K).

References

[1] C. H. Yang, D. Kan, and I. Takeuchi, Phys. Chem. Chem. Phys. **14**, 15953 (2012).
[2] M. H. Lee, D. J. Kim, J. S. Park, S. W. Kim T. K. Song, M. H. Kim, W. J. Kim, D. Do, and I. K. Jeong, Adv. Mater. **27**, 6976 (2015).
[3] T. Rojac, A. Bencan, B. Malic G. Tutuncu, J. Jones, J. Daniels, and D. Damjanovic, J. Ame. Cera. Socie. **97**, 1993 (2016).
[4] T. Zheng and J. G. Wu, J. Mater. Chem. C **3**, 684 (2015).
[5] Y. Qin, J. Yang, P. Xiong, W. Huang, J. Song, L. Yin, P. Tong, X. Zhu, and Y. Sun, J. Mater. Sci.: Mater. Electron. **29**, 7311 (2018).
[6] A. Prasatkhetragarn, P. Jantaratana, N. Vittayakorn, B. Yotburut, and R. Yimnirun, Ferroe. **451**, 109 (2013).
[7] Y. X. Wei, X. T. Wang, J. T. Zhu, and X. L. Wang, J. Am. Ceram. Soc. **96**, 3163 (2013).
[8] X. Z. Guo, Y. G. Wu, Y. N. Zou, and Z. Y. Wang, J. Mater. Sci.: Mater. Electron. **23**, 1072 (2012).
[9] D. Lebeugle, D. Colson, and A. Forget, Phys. Rev. B **76**, 024116 (2007).
[10] Y. P. Wang, L. Zhou, and M. F. Zhang, Appl. Phy. Lett. **84**, 1731 (2004).